Journal of Fluids and Structures (1991) **5**, 113–126

HYDRODYNAMIC FORCES ACTING ON CYLINDERS OSCILLATING AT SMALL AMPLITUDES

A. W. TROESCH
Department of Naval Architecture and Marine Engineering, The University of Michigan, Ann Arbor, MI 48109, U.S.A.

AND

S. K. KIM
Department of Mechanical Engineering, Kon-Kuk University, Seoul, Korea

(Received 17 January 1990 and in revised form 30 July 1990)

The hydrodynamic forces resulting from small-amplitude harmonic oscillations of arbitrarily shaped cylinders are considered both experimentally and theoretically. The fluid is assumed to be initially at rest. The theoretical model assumes a laminar, nonseparating flow, where the in-line force has two components, one due to normal pressure stresses and one due to skin friction. In the limit of zero amplitude oscillations, comparisons between theory and experiment demonstrate that the nonseparating theoretical model captures the essential behavior of real fluid hydrodynamics. This is valid for a variety of shapes including sharp-edged bodies such as squares. Through model testing, it is possible to estimate an "effective eddy viscosity" which can then be used in conjunction with the theoretical laminar flow model to give empirical drag coefficients.

1. INTRODUCTION

AN IMPORTANT AREA OF HYDROELASTIC DYNAMICS is the hydrodynamic force acting upon structural members while they undergo relatively high frequency, small amplitude oscillations. Offshore engineering examples of this include local riser dynamics, vertical motions of tension-leg platforms (TLPs), or longitudinal motions of stiffly-moored vessels. These vibratory motions are due to a number of sources, but all may be characterized as responses of lightly damped systems where the viscous contribution to the small, but non-zero, damping is a significant part of the total system damping. In off-resonant conditions, the damping is unimportant and the response is primarily a function of the system inertia, the system stiffness, and the external system excitation. However, near or at resonance the large stiffness and inertia forces cancel, and the response is governed solely by the ratio of the excitation to the damping.

Historically, much of the effort to understand the hydrodynamics of this problem has concentrated on the flow associated with simple geometric shapes such as circles. There are many articles in the available literature that discuss the viscous forces on circular cylinders in oscillating planar flows. Two representative textbooks are Sarpkaya and Isaacson (1981) for offshore applications or Chen (1987) for reactor component design. In addition to the circular geometry, much of the previous work was also limited to moderate Keulegan–Carpenter number and moderate Reynolds number flows. Relatively little consideration had been given to the hydrodynamic force in the flow regime characterized by small amplitude and large frequency. See Sarpkaya (1984, 1986) for example, where three types of flow transitions at low Keulegan–Carpenter number

0889–9746/91/010113 + 14 $03.00

were investigated: turbulence, vortex shedding and the Honji instability. Sarpkaya also examined the resulting behavior of the drag and inertia coefficients for a circular cylinder at Keulegan–Carpenter numbers less than 4. In another recent work, Bearman *et al.* (1985) considered vortex shedding effects on drag coefficients for sharp-edged bodies such as square cylinders. In those experiments and calculations, the Keulegan–Carpenter numbers varied between 1 and 4 and the flow was assumed laminar.

Due to difficulties associated with damping force measurements, there has been little data for drag coefficients at large Reynolds number where the Keulegan–Carpenter number is less than 1. The purpose of this paper is to show how drag and inertia coefficients vary as a function of cylindrical cross-section when the amplitude of oscillation approaches zero. Comparisons between previously published experimental results and those shown in this paper are discussed. Simularities, as in the case of the circular cross-section, and differences, as in the case of the square cross-section, are noted. The experimental technique described herein introduced a system resonance where a variable system stiffness approximately canceled the total system inertial force. The force measurement was then comprised primarily of the damping force. As a result, the experiments were able to produce reliable data points in the low Keulegan–Carpenter number range. Comparisons between these experimental measurements and a laminar, non-separating theory are also presented and discussed.

2. THEORETICAL PRELIMINARIES

Consider a two-dimensional body oscillating with known frequency Ω and amplitude A_0 in an incompressible Newtonian fluid. The fluid is initially assumed to be at rest. This is kinematically equivalent to the problem of a stationary cylinder in an oscillatory-free stream and only dynamically different from that problem by the pressure gradient force which is in phase with the acceleration. This acceleration force can be found by integration of the pressure gradients of the onset flow over the body contour. Assume that the flow resulting from the unsteady body boundary condition is laminar and that separation does not take place. These assumptions lead to the classical streaming flow problem investigated by Faraday (1831), Schlichting (1932), Holtzmark *et al.* (1954), Stuart (1966), Riley (1965), and Wang (1968) among others. Generally, these authors used a circular body geometry, and the resultant absence of separated flow seemed reasonable. More recently, Kim & Troesch (1989) applied the same set of assumptions to noncircular two-dimensional sections, including conformally mapped Lewis Forms (1929) and squares.

The traditional nondimensional numbers which determine the flow characteristics are defined as follows:

- Reynolds number: $$\mathrm{Re} = \frac{U_0 L}{\nu}$$
- Keulegan–Carpenter number: $$\mathrm{KC} = \frac{U_0}{L T_m} = \frac{2\pi A_0}{L}$$
- Frequency parameter: $$\beta = \frac{\mathrm{Re}}{K_c} = \frac{f L^2}{\nu}$$

where L is a length dimension of the two-dimensional cylinder, $\Omega = 2\pi f$ is a circular frequency, T_m is a period of the oscillation and $U_0 = \Omega A_0$. Only two of these numbers are independent.

Using experiments and theory, Kim & Troesch (1989) found that in the limit of zero KC the flow remained attached in a mean sense, even for sharp-edged bodies such as squares. Vortex shedding on the time scale of the streaming flow was not present. This conclusion was reached through the comparison of time lapsed flow visualizations and computed theoretical streamlines. The theoretical model developed by Kim & Troesch (1989) followed Wang (1968) and Davidson & Riley (1972), where the flow regime was separated into inner and outer regions. The reader is referred to that paper for the details on the theoretical model. Briefly, in the inner region, the flow was assumed to be governed by the classical Stokes boundary layer equation. In the outer region, the full Navier–Stokes equation for the steady streaming flow was solved numerically by using a finite difference method coupled with conformal mapping techniques.

Under the assumptions and conditions described by Kim & Troesch (1989), the flow in the inner region, up through first-order, can be represented by the outer potential flow and the *Stokes layer* where the flow is assumed to be attached. While the zero-order inviscid outer solution gives only the inertia force component at the basic frequency, the first-order boundary layer solution and first-order correction to the potential flow produce both inertia and drag force components whose nondimensional force coefficients are of $O(\beta^{-1/2})$. To this order, there is no effect due to the curvature or streaming flow, other than that present in the first-order potential calculations (Wang 1968).

The theoretical drag force has two sources, normal pressure and skin friction. These components are found to be equal for arbitrary two-dimensional bodies (Bearman *et al.* 1985). From the results of Bearman *et al.* (1985), the force computed from the Stokes layer solution, F_{BL}, is represented by

$$F_{BL} = \frac{1+i}{(\pi\beta)^{1/2}} \rho\Omega D \oint_S u_p \, dz, \tag{1}$$

where D, the body diameter, replaces the length scale, L, defined earlier and u_p is the potential tangential velocity on the body surface. The body boundary condition has a sinusoidal time dependence given by $e^{i\Omega t}$.

Conformal mapping offers a convenient way to get closed form expressions for u_p. The nomenclature used to define the mapping functionals and variables are given as $z = f(\zeta) = X + jY$, $\zeta = e^{ju}$ and $\Theta = \frac{\pi}{3} - \theta + \arg[f'(\zeta)]$.

For a conformally transformed body, u_p is given as

$$u_p e^{-j\Theta} = -\frac{dw}{dz} = -\frac{dW}{d\zeta}\frac{d\zeta}{dz}, \qquad u_p = -\frac{dW}{d\zeta}\frac{d\zeta}{dz} e^{j\Theta}, \tag{2}$$

where $W(\zeta)$ is a complex velocity potential in the computational domain, $w(z)$ is the corresponding one in the physical domain, and $j^2 = -1$. Equation (1) becomes

$$F_{BL} = -\frac{1+i}{(\pi\beta)^{1/2}} \rho\Omega D \oint_S \frac{dW}{d\zeta}\frac{d\zeta}{dz} e^{j\Theta} \, dz,$$

or (3)

$$F_{BL} = -\frac{1+i}{(\pi\beta)^{1/2}} \rho\Omega D \oint_S \frac{dW}{d\zeta} e^{j\Theta} \, d\zeta.$$

Now define various nondimensional force coefficients. The drag and inertia coefficients per unit length are

$$C_d = \frac{\mathcal{R}e\{F_{BL}\}}{\frac{1}{2}\rho U_0^2 D}, \qquad C_m = \frac{\mathcal{I}m\{F_p + F_{BL}\}}{\rho\Omega U_0 S_1}, \tag{4}$$

respectively, where F_p is the inertial force due to the zeroth order potential flow and S_1 is the cross-sectional area of the cylinder. To compare with the published results based upon the Morrison equation, (Sarpkaya & Isaacson 1981), drag and inertia coefficients are introduced as follows:

$$\bar{C}_d = \frac{3\pi}{8}\frac{\mathcal{R}e\{F_{BL}\}}{\frac{1}{2}\rho U_0^2 D}, \qquad \bar{C}_m = \frac{\mathcal{I}m\{F_p + F_{BL}\}}{\frac{\pi}{4}\rho\Omega U_0 D^2}, \tag{5}$$

where the Morrison equation is

$$F = \tfrac{1}{2}\rho U \mid U \mid D\bar{C}_d + \tfrac{\pi}{4}\rho D^2 \frac{dU}{dt}\bar{C}_m. \tag{6}$$

2.1. Hydrodynamic Force on a Circular Cylinder

Omitting $e^{i\Omega t}$, u_p and F_p are

$$u_p = 2U_0 \sin\theta$$

and

$$F_p = \tfrac{1}{2}\rho\Omega U_0 \pi D^2.$$

From equation (1), the force due to the boundary layer is

$$F_{BL} = \frac{1+i}{(\pi\beta)^{1/2}}\rho\Omega D\int_0^{2\pi} 2U_0 \sin^2\theta \frac{D}{2}\,d\theta = (1+i)\rho\Omega U_0 D^2\left(\frac{\pi}{\beta}\right)^{1/2}$$

and the corresponding force coefficients are

$$\begin{aligned} C_d &= 4\pi^{3/2}\mathrm{KC}^{-1}\beta^{-1/2}, \qquad C_m = 2 + 4(\pi\beta)^{-1/2}, \\ \bar{C}_d &= \tfrac{3}{2}\pi^{5/2}\mathrm{KC}^{-1}\beta^{-1/2}, \qquad \bar{C}_m = C_m. \end{aligned} \tag{7}$$

The values compare well with experiments in the laminar flow range, as shown by Bearman *et al.* (1985) and Sarpkaya (1984, 1986).

2.2. Hydrodynamic Force on a Lewis-Form Cylinder

Introduce a Lewis Transformation (Lewis 1929) of the form

$$z = \zeta + \frac{b}{\zeta^3}.$$

In order to have the same potential velocity, U_0, at infinity in both the physical and computational domains, consider a slightly different form of the mapping function. This form maps a Lewis-form cylinder with width D into a circle with diameter $d_0 = DR^*$, where the aspect ratio, R^*, is obtained by

$$R^* + \frac{b}{R^{*3}} = 1.$$

Body shapes that correspond to $b = -0{\cdot}04$, $-0{\cdot}06$, $-0{\cdot}08$, $-0{\cdot}10$, $-0{\cdot}12$ and the rounded square used in the forced oscillation experiments (solid line) are depicted in Figure 1.

With a known complex potential, $W = U_0(\zeta + \frac{1}{\zeta})$, where $\zeta = re^{j\theta}$, the derivatives become

$$\frac{dW}{d\zeta} = -2U_0 \sin\theta j e^{-j\Theta}$$

and

$$d\zeta = je^{j\theta}d\theta.$$

After substitution of these into equation (3), the force is then represented by

$$F_{BL} = -\frac{2(1+i)}{(\pi\beta)^{1/2}}\int_0^{2\pi} \sin\theta(\cos\Theta - j\sin\Theta)R^*\frac{D}{2}d\theta = -\frac{(1+i)}{(\pi\beta)^{1/2}}\rho\Omega D^2 U_0(I_1 + jI_2),$$

where

$$I_1 = R^*\int_0^{2\pi} \sin\theta\cos\Theta\, d\theta, \qquad I_2 = R^*\int_0^{2\pi} \sin\theta\sin\Theta\, d\theta = 0.$$

Let $I_b = I_1/\pi$ and the ratio between the area of a Lewis form and the area of a circle be

$$S_b = R^* - \frac{3^{1/2}b}{R^{*3}}.$$

From these results, the force coefficients are

$$\begin{aligned} C_d &= 4\pi^{3/2}\mathrm{KC}^{-1}\beta^{-1/2}I_b = I_b[C_d]_{\text{circle}}, \qquad C_m = 2 + \frac{4I_b}{(\pi\beta)^{1/2}}\frac{1}{S_b}, \\ \overline{C}_d &= \tfrac{3}{2}\pi^{5/2}\mathrm{KC}^{-1}\beta^{-1/2}I_b, \qquad \overline{C}_m = 2{\cdot}41 + \frac{4I_b}{(\pi\beta)^{1/2}}. \end{aligned} \tag{8}$$

force coefficients and values of I_b for the Lewis-forms with values of b varying from 0·0 to $-0{\cdot}13$ are given in Table 1. The coefficients are normalized with respect to KC and β. Presented in this form, comparisons can readily be made with experiments where both KC and β change.

The different shape types used in theory and experiments, Lewis forms and rounded square, were selected for ease in computation and manufacture, respectively. While

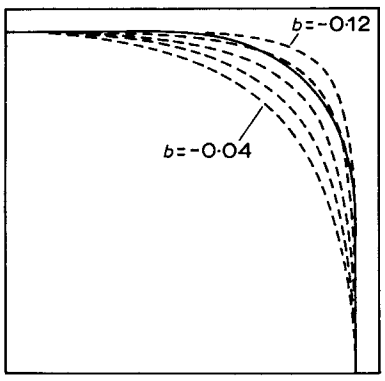

Figure 1. Bodies generated by the Lewis transformation with $b = -0{\cdot}12$, $-0{\cdot}10$, $-0{\cdot}08$, $-0{\cdot}06$, $-0{\cdot}04$ (in dashed lines); ——, body used in the experiments.

TABLE 1
Force coefficients for various shaped bodies

Shape	b	I_b	S_b	$C_d\mathrm{KC}\sqrt{\beta}$	$\bar{C}_d\mathrm{KC}\sqrt{\beta}$	$(C_m-2)\sqrt{\pi\beta}$
Circle	0	1	1	22·273	26·24	4
Lewis	−0·01	1·0095	1·0265	22·485	26·489	3·934
form	−0·02	1·0180	1·0517	22·674	26·712	3·872
	−0·03	1·0256	1·0755	22·843	26·912	3·814
	−0·04	1·0322	1·0983	22·991	27·085	3·759
	−0·05	1·0381	1·1201	23·121	27·240	3·707
	−0·06	1·0414	1·1398	23·196	27·326	3·655
	−0·07	1·0472	1·1611	23·324	27·479	3·608
	−0·08	1·0505	1·1804	23·398	27·565	3·560
	−0·09	1·0531	1·1991	23·455	27·633	3·513
	−0·10	1·0548	1·2172	23·493	27·678	3·466
	−0·11	1·0557	1·2347	23·514	27·702	3·420
	−0·12	1·0558	1·2517	23·517	27·705	3·374
	−0·13	1·0551	1·2682	23·501	27·689	3·328
Square				23·68	27·89	3·339

the two shapes cannot be compared directly, the variation in the coefficients for the different Lewis forms is small (Table 1), indicating that the theoretical difference between the Lewis form results and rounded square would also be small.

2.3. HYDRODYNAMIC FORCE ON A SQUARE CYLINDER

Bearman *et al.* (1985) derived the force computed from the Stokes layer solution and that solution is briefly outlined here for completeness. Consider the Schwartz–Christoffel transformation for a square cylinder as shown in Figure 2.

The mapping function is

$$z = \int_0^{\zeta} \left(\frac{\zeta^2 - \zeta_E^2}{\zeta^2 - \zeta_F^2} \right) \mathrm{d}\zeta.$$

With $W(\zeta) = U_0\zeta$, equation (2) is now

$$F_{\mathrm{BL}} = -\frac{2(1+i)}{(\pi\beta)^{1/2}} \rho\Omega D U_0 \oint_S \mathrm{e}^{j\Theta(s)}\, \mathrm{d}\zeta,$$

where $\Theta(s)$ is the orientation of the body surface in the physical domain in the

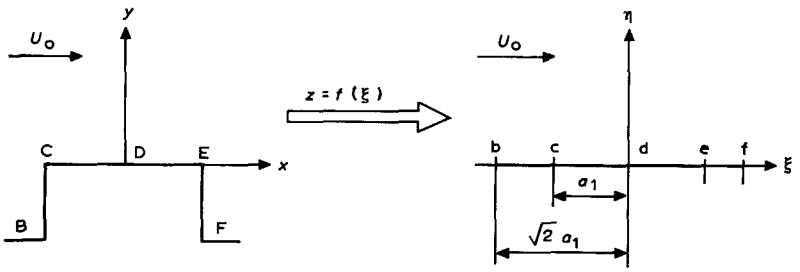

Figure 2. Schwartz–Christoffel transformation of the square cylinder.

tangential direction, s. Here, $\Theta = \pi/2$ for s between points B and C, and 0 for s between points C and D, as shown in Figure 2.

From symmetry arguments, the boundary layer force becomes

$$F_{BL} = -\frac{2(1+i)}{(\pi\beta)^{1/2}} \rho\Omega D U_0 \int_b^f e^{j\Theta}\, d\zeta = -4(\pi)^{1/2} \frac{(1+i)}{KC\,\beta^{1/2}} \rho U_0^2 D[2a_1],$$

where the constant a_1 is found to be 0·835.

Therefore, the force coefficients are

$$C_d = \pi^{3/2} a_1\, KC^{-1}\beta^{-1/2} \simeq 23{\cdot}68\, KC^{-1}\beta^{-1/2}, \qquad C_m = 2 + \frac{4a_1}{(\pi\beta)^{1/2}} \simeq 2 + 1{\cdot}884\,\beta^{-1/2},$$
$$\bar{C}_d = 27{\cdot}9\, KC^{-1}\beta^{-1/2}, \qquad \bar{C}_m = 2{\cdot}5465 + 2{\cdot}4\beta^{-1/2}. \tag{9}$$

These force coefficients are also included in Table 1.

3. EXPERIMENTAL FORCE MEASUREMENTS

Forced oscillation experiments using a vertical motion mechanism were conducted in the Ship Hydrodynamics Laboratory at The University of Michigan. The test cylinders were mounted horizontally between fixed end plates and oscillated vertically.

When oscillating a cylinder with small amplitude and large frequency, the inertia force dominates the force measurement, making it difficult to accurately determine the drag force. To briefly illustrate this, consider the forced vibration with known amplitude A_0 and frequency Ω. Assuming a linear system,

$$M\ddot{z} + b\dot{z} = F_0 e^{i(\Omega t + \delta)}, \qquad z = A_0 e^{i\Omega t},$$

or

$$[-M\Omega^2 + ib\Omega]A_0 = F_0 e^{i\delta}, \tag{10}$$

where M is a total system mass including added mass, b is the equivalent linear damping coefficient and δ is a phase lag. Digitized data of the force measurements can be transformed to give F_0 and δ by using the Fast Fourier Transform (FFT). Then M and b are found from equation (10):

$$M = -\frac{F_0}{A_0\Omega^2}\cos\delta, \qquad b = \frac{F_0}{\Omega A_0}\sin\delta. \tag{11}$$

For a lightly damped system, $b/M\Omega \ll 1$ and $\delta \simeq 180°$. Therefore, a small error in obtaining δ in the experiments results in a significant error in drag force estimates. In experiments, phase shift errors can exist due to mechanical load cells, signal processing, system damping, etc. These effects may be nonlinear and they significantly increase the difficulty in conducting experiments for $KC < 1$ with large β. This may be one of the principal reasons why previously published experimental results have significant scatter for small KC.

One experimental technique to overcome this difficulty is to introduce a spring that counteracts the inertial force of the system. That is, forced vibration experiments are run near the resonance frequency of the spring-mass-damper system. To control the natural frequency easily, a slender aluminum beam is employed as a spring. The approximate value of the resonant frequency is found by using the effective spring constant for a cantilever beam from simple slender beam theory,

$$k_{eff} = \frac{3EI}{L_{spring}^3} = M\Omega^2. \tag{12}$$

The beam mass and damping are ignored.

From equation (12), the system natural frequency can be controlled easily by changing L_{spring} and then fine tuned through trial and error by varying Ω in small increments to give $\delta \simeq 90°$. With the spring included in the equation of motion, the inertial and drag forces can easily be shown to be

$$F_I = k_{\text{eff}} A_0 - F_0 \cos \delta, \qquad F_d = F_0 \sin \delta, \tag{13}$$

where k_{eff} is the effective spring constant of the cantilever beam. To illustrate the effectiveness of this technique, consider a typical example, one which occurred frequently during the tests. Without the spring, a recorded $\delta = 179{\cdot}9$ with $0{\cdot}6°$ error in the measured phase angle gives an 66·7% error in the damping force. However, with the spring, δ might be 82° and the same error in the phase angle produces only a 0·15% error in the damping force. The experimental test apparatus was configured to maximize the effectiveness of this idea. Load cells were mounted on the spring and on the oscillating cylinder. Both the external exciting force, F_0, and the effective spring force, $k_{\text{eff}} A_0$, were measured directly.

Each experimental test run produced three data sets, a displacement, the force on the cylinder, and the force on the spring. Typically, the FFT analysis routine transformed data of ten periods of oscillation after a start-up of approximately ten periods. The sampling period of the A/D converter was adjusted for each run so that the time histories represented an integral number of cycles. Since the sampling period could be set to only three significant figures, ten cycles were collected to minimize leakage effects. The springs were made of 2·54 cm by 1·27 cm rectangular pieces of aluminum, varying in length from 42·5 cm to 76·8 cm. The lengths of the springs were adjusted so that $\beta = 23{,}200$ and 48,600 for the three test cylinders. The amplitude of the oscillator was adjusted to produce a range of KC from 0·079 to 0·58. The experimental test matrix is given in Table 2.

For the values of $\beta = 23{,}200$ and 48,600, the flow is turbulent (Sarpkaya 1984). Consequently, the theoretical laminar formulas for the inertial and drag coefficients, equations (7)–(9), cannot be compared directly with the experimental results. These large values of β were selected, however, since the turbulent experimental conditions represent those more likely to be encountered in full-scale ocean structures. Also, based upon Sarpkaya (1984), it was expected that the turbulent drag coefficients versus KC on log–log graph scales would have the same slope as the laminar flow condition.

Experimental results for a circular cylinder of 20·3 cm in diameter and 1·82 m in length are depicted in Figures 3 and 4. Results for a rounded square are given in Figures 5 and 6. The rounded square was manufactured from a 1·82 m long cylinder with a 15·2 cm by 15·2 cm cross-section. The radius of the corner rounds was 5·1 cm. The geometry is shown in Figure 2. Results for a square cylinder are depicted in Figures 7 and 8. In these figures, C_m and C_d are the inertia and drag coefficients which

TABLE 2
Test matrix for forced oscillation experiments

Shape	β	KC range	Period (s)
Circular cylinder	48,600	0·095–0·51	0·85
	23,200	0·098–0·2	1·78
Rounded square	48,600	0·079–0·51	0·85
cylinder	23,200	0·11 –0·58	1·78
Square cylinder	48,600	0·079–0·51	0·85
	23,200	0·079–0·58	1·78

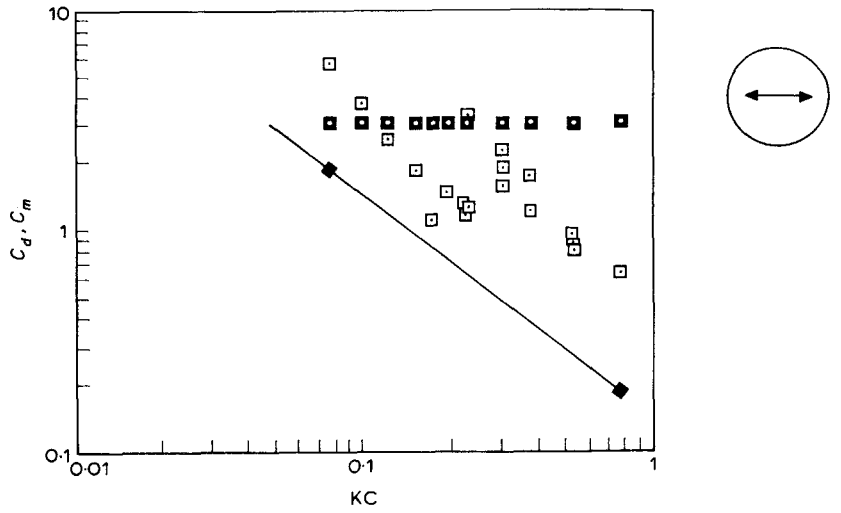

Figure 3. Drag and inertial coefficients of a circular cylinder with $\beta = 23{,}200$; □, C_d; ◆, laminar flow C_d; ■, C_m.

are defined in equation (4). $C_{d\,\text{laminar}}$ denotes the theoretical value of the drag coefficient for laminar flow, shown in equations (7), (8) and (9). These results are discussed and compared with theory in the next section.

4. RESULTS AND DISCUSSION

Based on the experimental results of Sarpkaya (1984, 1986), Bearman (1984) and Bearman *et al.* (1985), a harmonically oscillating cylinder in calm water or a stationary cylinder in a harmonically oscillatory onset flow, produces a drag coefficient line which can exhibit three types of flow transitions; KC_t, transition from laminar flow to turbulent flow, KC_v, onset of vortex shedding, and KC_{cr}, inception of "the Honji

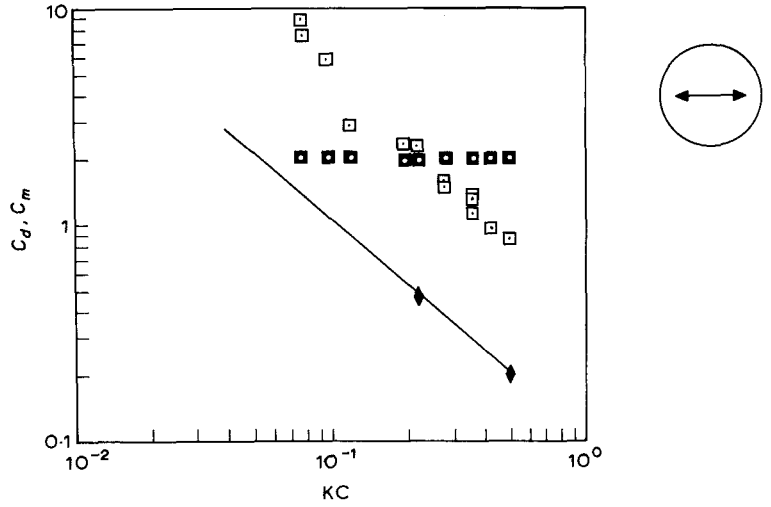

Figure 4. Drag and inertial coefficients of a circular cylinder with $\beta = 48{,}600$; □, C_d; ◆, laminar flow C_d; ■, C_m.

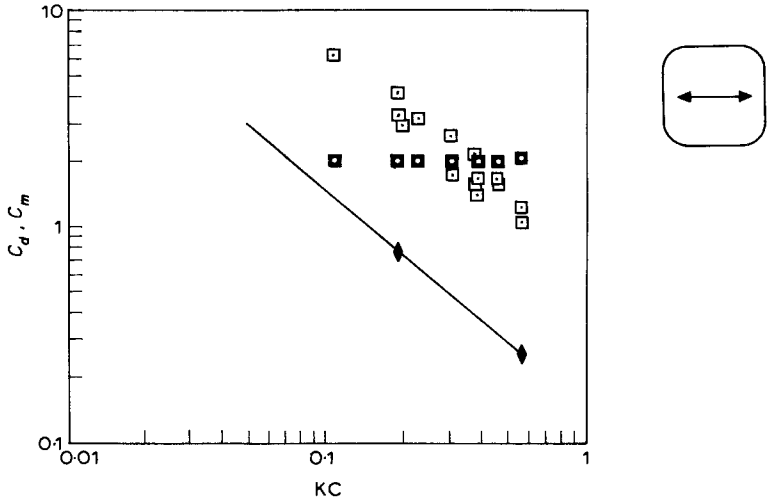

Figure 5. Drag and inertial coefficients of a rounded square cylinder with $\beta = 23{,}200$; □, C_d; ◆, laminar flow C_d; ■, C_m.

Vortical Instability". The last transition occurs only for a vertically mounted cylinder where the gravity effects in line with the cylinder axis become important. This type of instability is therefore not relevant to the horizontally mounted cylinders described in this work. In this section, the results of the forced vibration experiments are discussed and compared with the laminar, nonseparating theoretical calculations.

4.1. Circular and Rounded Square Cylinders

There is no evidence of vortex shedding when $KC < 0{\cdot}6$ for $\beta = 23{,}200$ or 48,600 for both cylinders. In turbulent flow, onset of vortex shedding is initiated at a larger KC than in laminar flow, typically at $KC \geq 3$ for $\beta = O(10^4)$ (Sarpkaya 1986). Therefore, the experimental drag coefficients form lines parallel to the theoretical drag coefficient

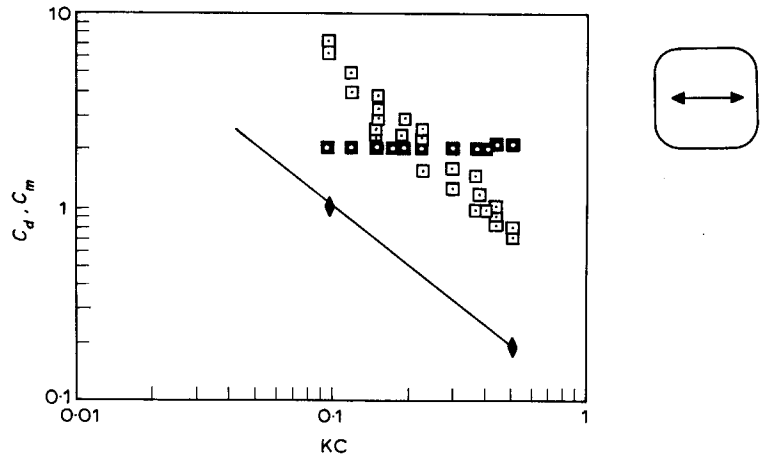

Figure 6. Drag and inertial coefficients of a rounded square cylinder with $\beta = 48{,}600$; □, C_d; ◆, laminar flow C_d; ■, C_m.

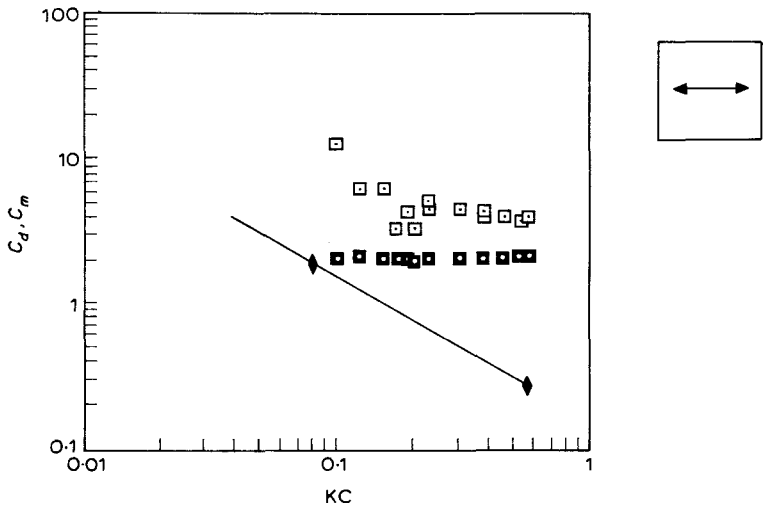

Figure 7. Drag and inertial coefficients of a square cylinder with $\beta = 23{,}200$; □, C_d; ◆, laminar flow C_d; ■, C_m.

lines of laminar flow (Wang 1968) or equations (7) and (8) as depicted in Figures 3–6. Their magnitudes, however, are about 4·5 times greater than the theoretical ones. Bearman, in Sarpkaya's paper (1984), suggested that if β is formed using an *effective eddy viscosity,* then the experimental and theoretical values of the drag coefficient may be made to coincide for $KC_t < KC < KC_v$ at large β. In Sarpkaya's U-tube experimental results for a smooth circular cylinder, the ratio between the eddy and kinematic viscosities, ν_t/ν, was about 25 : 1. The experimental results presented here require that ν_t/ν be approximately 20 at $\beta = 23{,}200$ and 48,000. In addition, the cylinders used in this work were mounted horizontally and were oscillating in calm water, while the free stream was oscillating in Sarpkaya's experiments. A possible explanation for the relatively smaller eddy viscosity at higher β is that the present experiments had less free stream turbulence and no Honji instability.

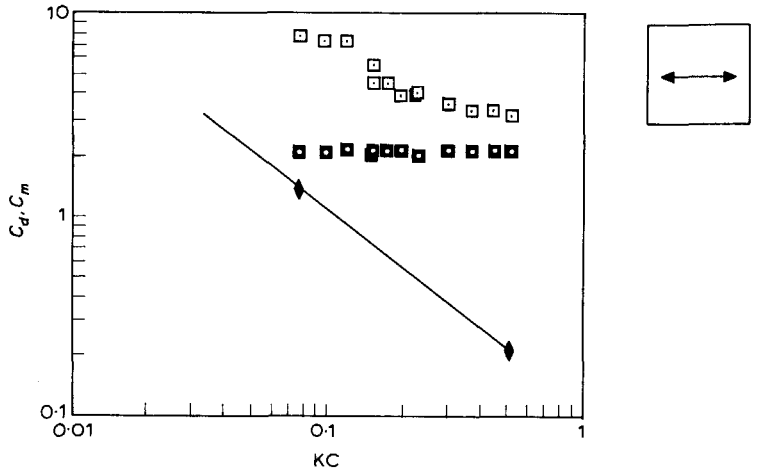

Figure 8. Drag and inertial coefficients of a square cylinder with $\beta = 48{,}600$; □, C_d; ◆, laminar flow C_d; ■, C_m.

From comparison of Figures 3 and 4 to Figures 5 and 6, it is clear that the drag coefficients for a rounded square have nearly the same slope as that of a circular cylinder, with only a small difference in magnitudes. This may have been anticipated, since the amplitude of oscillation is smaller than the radius of curvature of the corners in the rounded square, and consequently separation should not occur (Batchelor 1973). The small difference is also consistent with the theoretical values given in Table 1. In the limiting case for $KC \rightarrow 0$, a theory that does not include vortex shedding appears valid for bodies with increasingly sharp edges. One hydrodynamic difference between the two shapes is that transition to turbulent flow seems to occur at smaller KC for the rounded square cylinder. Actual data at $\beta = 23{,}200$ and $KC < 0{\cdot}2$ are scattered for the circular cylinder because the transition to turbulent flow may happen around $KC = 0{\cdot}07$–$0{\cdot}2$, $Re_t \simeq 1{,}000$–$2{,}000$ (Sarpkaya 1984). Data for the rounded square, however, are not as scattered.

When eddy viscosity is included, inertia coefficients for both shapes display trends shown by the theoretical values determined from equations (7) and (8). These trends indicate that viscosity acts to slightly increase the inertial coefficient over its potential-flow value of 2·0. As can be seen in Figures 3–6, most of the experimental values are between 2·03–2·09, while the theoretical values are 2·015 at $\beta = 23{,}200$ and 2·01 at $\beta = 48{,}600$. If β is formed using an eddy viscosity, then the theoretical inertia coefficient is approximately 2·05. Inertia coefficients also increase very slowly with increasing KC.

4.2. Square Cylinder

The experimental drag coefficient data with two theoretical reference lines are shown in Figure 9. One solid line (left, with the larger negative slope) is parallel to the theoretical values, given in equation (9) and the other (right, with the smaller negative slope) is parallel to the theoretical values obtained including the effect of vortex shedding by using the inviscid shedding model of an isolated edge (Bearman *et al.* 1985). The theoretical values for the drag coefficients based upon the vortex shedding model are denoted as squares.

Through comparison of Figures 7, 8 and 9 with the results of Bearman *et al.* (1985), it is clear that for a square cylinder with sharp edges at large β there exists a region free

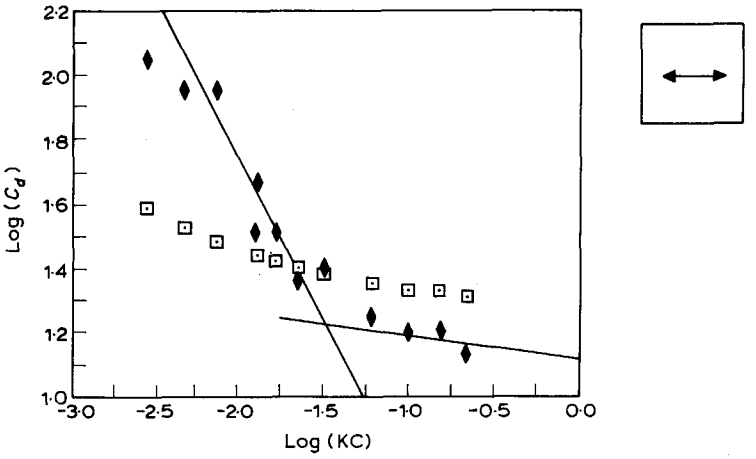

Figure 9. Transition in the drag coefficient of a square cylinder; □, Bearman *et al.* (1985), ◆, Log(C_d).

of vortex shedding ($KC \leq 0{\cdot}2$). The drag coefficient based upon the theoretical vortex shedding model shows only a moderate dependence upon KC, while the theoretical unseparated flow, nonvortex shedding model shows a larger dependence upon KC. The experiments indicate that the transition from one of these models to the other occurs at approximately $KC = 0{\cdot}2$. This implies that KC_t is smaller than KC_v and that in a real fluid, the assumption of ignoring vortex shedding at small KC for streaming type flow seems to be valid. This statement would not be true if there were an initial uniform stream.

The ratio between the eddy and laminar viscosity, ν_t/ν, is about 50, which is a much larger ratio than that of the other two shapes at $KC \leq 0{\cdot}2$ and $\beta = 48{,}600$. This implies that shape is important even when vortex shedding is not present due to the increased turbulence level associated with a sharp-edged body at large β.

Inertia coefficients for a square cylinder have values that are almost constant, around 2·05–2·13. These agree well with the theoretical values predicted by equation (9), which is about 2·01 for laminar flow, or 2·06 if the eddy viscosity is introduced. Both experiment and theory show that viscous effects increase the value of the inertial coefficients over the potential-flow value by a few per cent.

5. CONCLUSION

The hydrodynamic inertia and drag forces resulting from small-amplitude harmonic oscillations of a circle, rounded square, and square have been determined both experimentally and theoretically. The results are valid for small, near-zero values of KC and large values of β.

For a sharp-edged cylinder, such as a square cylinder, the transition from laminar to turbulent flow for fixed β occurs at smaller KC than the onset of vortex shedding. As β increases, the onset of vortex shedding occurs at relatively larger KC. For a value of $\beta = O(10^4)$, vortex shedding for an oscillating square cylinder occurs at approximately $KC = 0{\cdot}2$.

The theoretical model for the shapes tested, assumes a laminar, nonseparating flow. The drag force at small KC is proportional to the amplitude of oscillation. As a result, the drag coefficient line, when plotted on a log-scaled C_d versus KC graph, has the same slope, but not intercept, as that of the experiments. The experimental results have made it possible to estimate effective eddy viscosities which can be used in conjunction with the theoretical laminar flow model to give empirical drag coefficients. The inertia coefficients obtained using these values of the eddy viscosity also compare well with the experimental results.

ACKNOWLEDGMENTS

This work was supported by The University of Michigan/Sea Grant/Industry Consortium in Offshore Engineering under the Michigan Sea Grant Program, project numbers E/GLE-14 and R/T-23, under grant number NA85AA–SG045C from the Office of Sea Grant, National Oceanic and Atmospheric Administration (NOAA), U.S. Department of Commerce, and funds from the State of Michigan. Industry participants include the American Bureau of Shipping; Conoco, Inc.; EXXON Production Research; Friede and Goldman, Ltd.; Nobel, Denton and Associates, Inc.; Shell Companies Foundation (1985–1986); and the U.S. Coast Guard.

References

BATCHELOR, G. K. 1973 Section 5.13: Oscillatory boundary layers, in *An Introduction to Fluid Dynamics,* pp. 353–364. Cambridge: Cambridge University Press.

BEARMAN, P. W. 1984 Vortex trajectories in oscillatory flow. In *Proceedings on Separated Flow around Marine Structures,* The Norwegian Institute of Technology, Trondheim, Norway, pp. 133–153.

BEARMAN, P. W., DOWNIE, M. J., GRAHAM, J. M. R. & OBASAJU, E. D. 1985 Forces on cylinders in viscous oscillatory flow at low Keulegan–Carpenter Numbers. *Journal of Fluid Mechanics* **154,** 337–356.

CHEN, S. S. 1987 *Flow-Induced Vibration of Circular Cylindrical Structures.* Washington: Hemisphere Publishing Corporation.

DAVIDSON, B. J. & RILEY, N. (1972) Jets induced by oscillatory motion. *Journal of Fluid Mechanics* **53,** 287–303.

FARADAY, D. J. 1831 On a pecular class of acoustical figures, and on certain forms assumed by groups of particles upon vibrating elastic surfaces. *Philosophical Transactions of the Royal Society (London)* **121,** 299–340.

HOLTZMARK, J., JOHNSEN, I., SIKKELAND, T. & SKAVLEM, S. 1954 Boundary layer flow near a cylinder obstacle in an oscillatory flow. *Journal of Acoustical Society of America* **26,** 26–29.

KIM, S. K. & TROESCH, A. W. 1989 Streaming flows generated by high-frequency small-amplitude oscillations of arbitrarily shaped cylinders. *Physics of Fluids A,* **1,** 975–985.

LEWIS, F. M. 1929 The inertia of water surrounding a vibrating ship. *Transactions of the Society of Naval Architects and Marine Engineers (SNAME)* **37,** 1–20.

RILEY, N. 1965 Oscillating Viscous Flows. *Mathematika* **12,** 161–175.

SARPKAYA, T. & ISAACSON, M. 1981 *Mechanics of Wave Forces on Offshore Structures.* New York: Van Nostrand Reinhold.

SARPKAYA, T. 1984 Past process and outstanding problems in time-dependent flows about ocean structure. In *Proceedings on Separated Flow around Marine Structures,* The Norwegian Institute of Technology, Trondheim, Norway, pp. 1–36.

SARPKAYA, T. 1986 Force on circular cylinder in viscous oscillatory flow at low Keulegan–Carpenter numbers. *Journal of Fluid Mechanics* **65,** 61–71.

SCHLICHTING, H. 1968 Section on non-steady laminar boundary layers, in *Boundary Layer Theory,* pp. 408–434. New York: McGraw-Hill.

STUART, J. T. 1966 Double boundary layer in oscillatory viscous flow. *Journal of Fluid Mechanics* **24,** 274–297.

WANG, C. Y. 1968 On high-frequency oscillatory viscous flow. *Journal of Fluid Mechanics* **32,** 55–68.